We are IntechOpen, the world's leading publisher of Open Access books Built by scientists, for scientists

6,900
Open access books available

185,000
International authors and editors

200M
Downloads

Our authors are among the

154
Countries delivered to

TOP 1%
most cited scientists

12.2%
Contributors from top 500 universities



WEB OF SCIENCE™

Selection of our books indexed in the Book Citation Index in Web of Science™ Core Collection (BKCI)

Interested in publishing with us?
Contact book.department@intechopen.com

Numbers displayed above are based on latest data collected.
For more information visit www.intechopen.com



Chapter 15

Performance Assessment of UWB-Over-Fiber and Applications

João M.B. Oliveira, Luís M. Pessoa, Diogo Coelho, Henrique M. Salgado and Jorge C.S. Castro

Additional information is available at the end of the chapter

http://dx.doi.org/10.5772/48748

1. Introduction

Since 2002, the Federal Communications Commission (FCC) authorized the use of ultra-wideband (UWB) signal transmissions for unlicensed use, in the range from 3.1 to 10.6 GHz, leading to a revived interest in research activities and to new opportunities for companies to explore and develop new broadband indoor and outdoor applications [1]. Moreover, UWB is seen as a promising technology for short range high speed wireless networks.

UWB signals are characterized by their huge bandwidth occupancy, high data rates, and very weak power density (−41.3 dBm/MHz), which gives them a noise-like signal characteristic, facilitating both interference mitigation and very low device power consumption. On the other hand, its very low intensity and high data rates limit the coverage to a few meters distance. Yet, by using radio-over-fiber (RoF) as a signal transportation technique, it is possible to deliver UWB signals over a fiber based network.

The radio-over-fiber (RoF) concept involves the transmission of RF signals by an optical fiber between a control station (CS) and a number of base stations (BSs). In the base stations, the RF signal is transmitted to end users by a wireless link. Integration of both optical and wireless broadband infrastructures into the same backhaul network leads to a significant simplification and cost reduction of BSs since all routing, switching and processing are shifted to the CS. This centralization of signal processing functions enables equipment sharing, dynamic allocation of resources, and simplified system operation and maintenance. The concept of RoF is shown in Figure 1 in an in-building network context.

RoF systems are (ideally) transparent to all signals transmitted in the optical fiber. It has been experimentally shown that RoF networks are well suited to simultaneously transport several wireless standards like wideband code division multiple access (WCDMA), IEEE 802.11 wireless local area network (WLAN) [2], global system for mobile communications

INTECH
open science | open minds

©2012 Oliveira et al., licensee InTech. This is an open access chapter distributed under the terms of the Creative Commons Attribution License (http://creativecommons.org/licenses/by/3.0), which permits unrestricted use, distribution, and reproduction in any medium, provided the original work is properly cited.

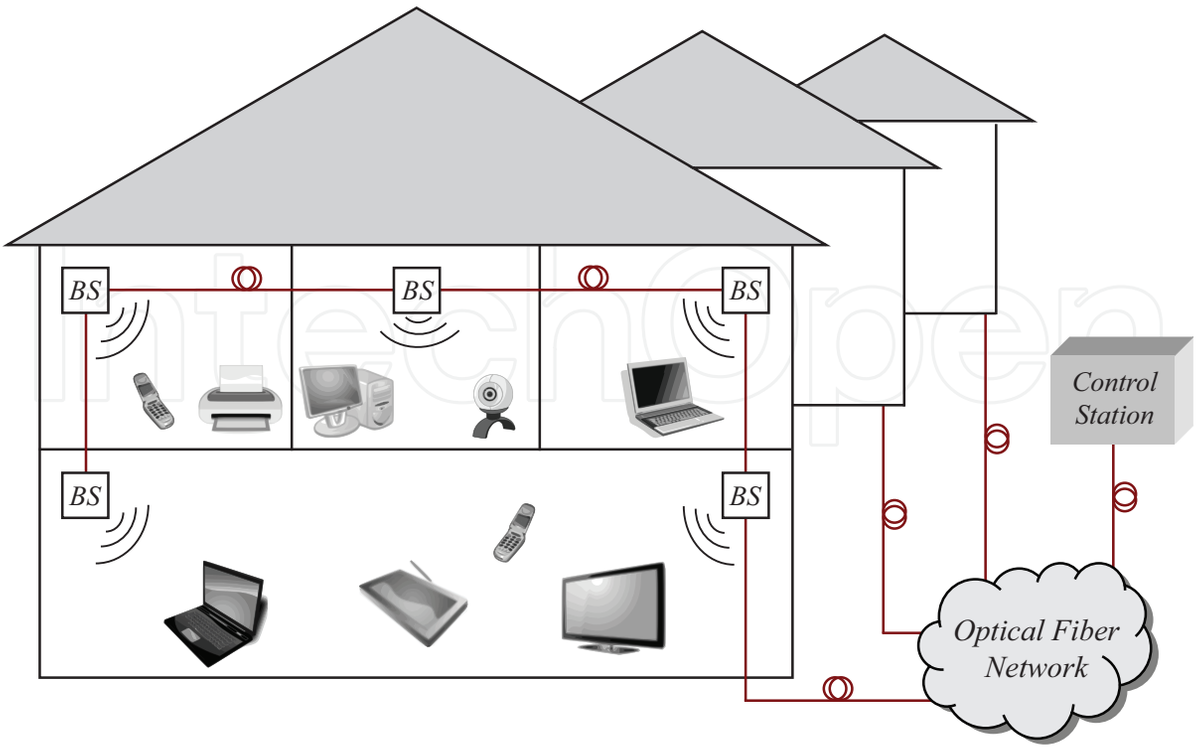


Figure 1. In-building radio-over-fiber concept.

(GSM) [3], WiMAX [4] and ultra-wide band (UWB) [5, 6]. Moreover, RoF systems also offer other attractive advantages such as low weight and immunity to electromagnetic interference. However, an optically modulated mm-wave signal can also suffer from several impairments namely nonlinear distortion, power penalty from the electric/optic/electric (E/O/E) conversion process, chromatic dispersion, attenuation from the optical fiber and phase noise from LASER sources.

Here we study the transmission performance of UWB over two distinctive optical networks. In Section 2, the packet error rate performnace in a low-cost multi-mode fiber (MMF) network composed by a 850 nm vertical-cavity surface emitting LASER (VCSEL) and a PIN photodiode connected by two different polymer optical fibers (POF) is assessed. Then, in Section 3, an analytical and experimental performance evaluation is carried out in a single-mode fiber (SMF) network composed by a reflective electro-absorption modulator (R-EAM) and a PIN photodiode.

2. UWB over perfluorinated graded index polymer optical fiber for low-cost in-building networks

The use of multimode fibers (MMF) in RoF short span networks has attracted much attention in recent years. Nowadays, the majority of building networks are based on MMF. In fact, in-building networks employing MMF topologies for high speed short-range (10 Gb/s; < 300 m) represent about 90% of all in-building networks [7]. Furthermore, it is predicted that the fastest growing part of the optical communications market will be targeting legacy MMF for installed lengths up to 300 meters.

Polymer optical fiber (POF) is an emerging medium for very short reach links. The popularity of polymer optical fiber is due to the advantages brought by its large core diameter and mechanical properties. These include connectorization simplicity due to the large numerical aperture, high tolerance to both misalignments and vibrations, low bending loss that eases installation and simple and low maintenance costs due to its robustness.

Common polymer optical fibers are based on polymethyl methacrylate (PMMA-POF). These fibers exhibit low bandwidth, multimodal dispersion and high attenuation (200 dB/km) hence are not suitable for today's high data rates or RoF systems where signals usually exhibit high bandwidths and high RF frequency carriers. Due to their relatively low bandwidth, a down-conversion of the RF signal to an intermediate frequency would be necessary, which introduces additional complexity and raises the cost of the BSs. Newer perfluorinated graded index polymer optical fiber (PF-GI-POF) from companies such as Sekisui Chemical, Chromis Fiber or Asahi Glass, solve this issue by combining a low attenuation material (about 50 dB/km @ 850 nm) with a graded index profile in their fiber construction. Bandwidth is relatively high for graded-index multimode fibers. Current PF-GI-POFs have bandwidth length products of around 1 GHz·Km, and attenuations as low as 10 dB/Km at 1310 nm [8]. In practical terms, for short links (< 100 m), it is limited by the response of directly modulated laser devices [9].

Comparing to common silica multimode fiber (SI-MMF) with respect to transmission capacity, PF-GI-POF has the potential of high bandwidth and a lower modal dispersion. Moreover, it offers lower material dispersion and higher bandwidth than standard MMF with 40 Gb/s data transmission capability for 100 m links [9].

The attenuation is not an issue for short silica-based fiber link lengths. But in the case of POF the attenuation can be as high as 20 dB for the PMMA-POF or about 5 dB for the state of the art PF-GI-POF for a 100 m length link. Large-core glass fiber shows lower attenuation than POF, however their core size is restricted to 200 μm due to the inherent inflexibility of glass. In this situation, POF again has advantages concerning easy handling and termination, tolerance to misalignments and high mechanical strength [10]. Furthermore, the typical large core of polymer fiber allows for large tolerance on misalignments that results in the possibility of using cheaper connectors. For comparison, consider the case of the power loss due to lateral (axial) misalignment of connecting two graded index (parabolic case) MMF with different core diameters. Comparing the power loss, assuming uniformly modal power distributions, for a misalignment of 25 μm, yields a loss of 1.76 dB for a 62.5 μm core diameter MMF whereas for the case of POF with a core diameter of 200 μm, the same 25 μm displacement results only in 0.48 dB loss [11]. New PF-GI-POF fibers being developed are able to withstand large temperature variation (-65 C to 125 C) and so may be suitable for applications in harsh critical environments. Their ease of installation, and tolerance to misalignment, vibration and large temperature variation operation makes these fibers suitable for short-range applications in the home environment or in critical applications such as the car and the avionics industry.

Here, we experimentally demonstrate the uplink of a MB-OFDM UWB signal (ECMA-368 standard [12]) over two different PF-GI-POFs from Chromis Fiberoptics using commercial UWB transceivers and cheap commercial off-the-shelf (COTS) components, namely an optical transceiver composed by a low-cost 850 nm VCSEL and a PIN photodiode.

2.1. A low-cost directly modulated RoF system

VCSELs are characterized by a vertical low divergence, circular beam patterns, low threshold currents (a few mA) and high bandwidths (several GHz). Their vertical wafer growth process enables in-wafer testing, and is well suited for large scale production. Their output light beam pattern enables efficient coupling to large diameter polymer optical fibers. Hence, simple plastic injection molded packages are sufficient as fiber coupling devices. These are reasons that make VCSELs desirable for low cost directly modulated systems in these types of widespread commercial applications.

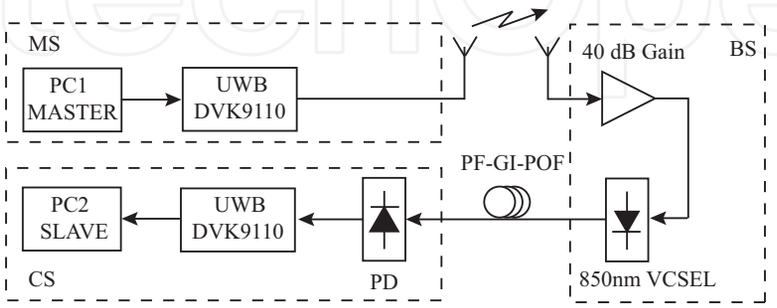


Figure 2. Schematic illustrating the RoF setup used.

A schematic of the MB-OFDM UWB over GI-POF system used is shown in Figure 2, representing a RoF communication uplink between a Mobile Station (MS) and a Control Station (CS), via a Base Station (BS). In order to generate MB-OFDM UWB signals compliant with the ECMA-368 standard, a commercially available UWB transceiver module from WisAir (DVK9110M) was used. The proposed system is based on today's commercially available low cost VCSELs and photodiodes that are not optimized for radio-over-fiber applications.

At the BS, a power amplifier (PA) amplifies the driver signal. The optical signal power (P_{OPT} in dBm) at the laser output is given by [13, 14]

$$P_{OPT} = \frac{G_{TX} + P_{RF,BS}}{2} + 10\log_{10}\left(G_M\sqrt{\frac{1000}{Z_{in}}}\right) \tag{1}$$

where G_{TX} is the PA gain in dB, $P_{RF,BS} = P_{RF,MS} - L$ is the received electrical power (in dBm) at the BS, $P_{RF,MS}$ is the transmitter electrical power at the MS, L is the wireless link loss, G_M is the VCSEL modulation gain (or slope sfficiency) in mW/mA and Z_{in} ($\sim$50 Ω) is the laser input impedance assumed constant within the band of interest.

The received electrical power at the CS, $P_{RF,CS}$, is given by

$$P_{RF,CS} = 20\log_{10}(RG_M) + 10\log_{10}\left(\frac{Z_{out}}{Z_{in}}\right) - 2OL + G_{TX} + P_{RF,MS} - L \tag{2}$$

where R is the photodiode responsivity in mA/mW, Z_{out} ($\sim$50 Ω) is the photodiode output impedance (also assumed constant within the band of interest) and OL is the optical power loss due to both the fiber attenuation and connector loss. Note the factor of 2 multiplying the optical power term which results from the quadratic optical power to electrical power

conversion in the photodiode meaning that reduction on the transmitted optical power has a significant impact on the link budget.

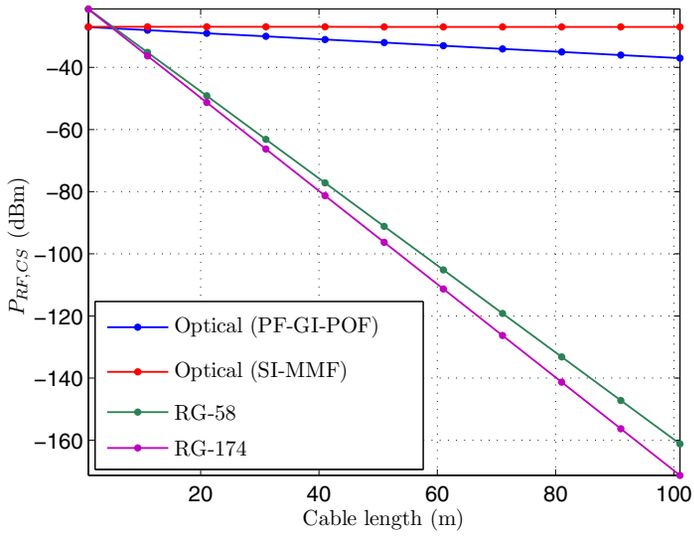


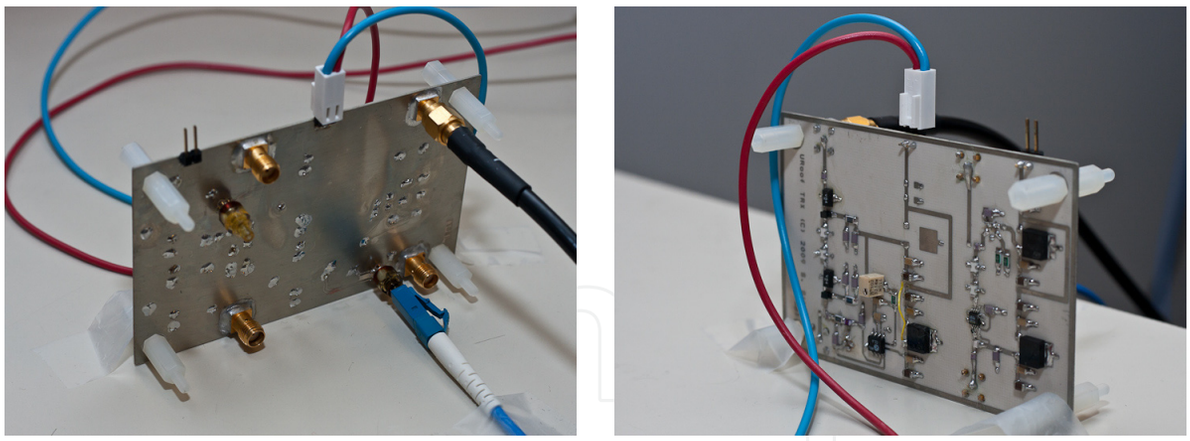
Figure 3. RF power at the CS as a function of the cable length.

Figure 3 shows the RF power at the CS as function of the cable length. For this illustrative result, we consider an UWB signal transmission over the setup given by Figure 2 with the following specifications: $P_{RF_MS} = -19.7$ dBm, a wireless link of 1 meter ($L \approx 40$ dB), $RG_M = 0.88$, $G_{TX} = 40$ dB and $Z_{out} \approx Z_{in} = 50\Omega$. We compare this result with the loss of common silica multimode fiber (SI-MMF) and RF electrical cables (RG-58 and RG-174 considering the same operating band and the same RF gain as applied to the E/O/E converter). Although there is a penalty by using the E/O/E conversion and optical transport, this is nonetheless very small when compared to the loss suffered by the signal when transported with electrical cable at distances of several tens of meters. It can be seen that the electrical to optical and optical to electrical conversion (whose efficiency is given by RG_M) jointly with the attenuation of POFs is the dominant factor reducing the link power budget of these systems. The relatively high POF attenuation can be partially overcome by post detection amplification, at the expense of some SNR degradation due to amplifier noise. In our experiments, an extra LNA was not included because the UWB DVK provides enough sensitivity.

MB-OFDM UWB radio applications make extensive use of multiple subcarriers and, hence require large dynamic range and highly linear devices. The signal transmission is mainly impaired by the laser nonlinearity, the optical loss due to the fiber, the free space loss and noise added by the system.

2.2. Experimental demonstration of concept

Figure 4 depicts the RoF conversion board based on low-cost electrical and optical components. An amplifier cascade and a polarizing circuit makes up the laser driver for the E/O conversion circuit and a photodiode with an integrated transimpedance amplifier was used for the O/E conversion circuit.



(a) Top view. (b) Bottom view.

Figure 4. RoF conversion board used as E/O/E transceiver.

The amplifiers were chosen among devices with both high IP3 (3rd Order Intercept) and low noise figure. High IP3 is essential for guaranteeing the integrity of multiple carrier ultra wideband signals. The VCSEL (HFD3180-203) and photodiode (HFE4192-581) operate at 850 nm, and have a combined 3 dB bandwidth of about 5 GHz. The laser modulation efficiency, and photodiode (PD) responsivity are 0.07 mW/mA and 12.5 mA/mW, including transimpedance amplifier gain, respectively. It was also experimentally verified that the receiver noise is much larger than the laser RIN, even with short POF lengths.

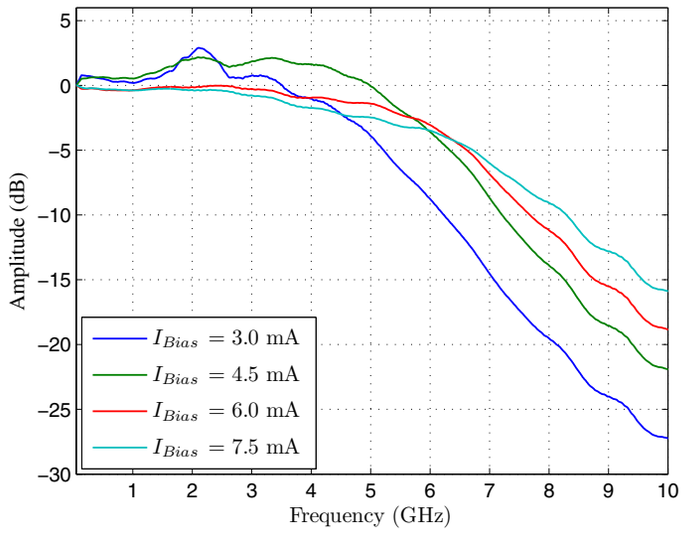


Figure 5. VCSEL transfer function vs. DC bias current.

The VCSEL bias current was also judiciously adjusted. It was found that the current that provides the maximum bandwidth (6 − 7.5 mA, see Figure 5) is not the one corresponding to the optimum operation point. Instead, the bias current was set to the lower level of 4.5 mA, which increases the output optical modulation index (the input RF intensity is fixed), without significantly compromising the bandwidth, and without significantly increasing the laser nonlinear dynamic distortion.

The total budget of this system prototype does not exceed €50. Large scale production of such a system would undoubtedly have an even lower price, meeting well in the requirements of a widespread commercial application for home or office use.

The UWB kit operates is the band group 1 (from 3.168 GHz to 4.752 GHz) and the maximum equivalent isotropic radiated power (EIRP) is −41.3 dBm/MHz using antennas with approximately 4 dBi of gain. This band group consists of three sub-bands, each occupying a bandwidth of 528 MHz and containing 128 subcarriers. Consequently, the power transmitted by the UWB DVK is approximately −19 dBm, disregarding the antenna gain. Although three subbands are available for transmission, the optical transceiver design limitations (commercial VCSEL, photodiode and amplifiers available at the moment) prevented using the entire available bandwidth. Therefore, the time-frequency code was set to TFC 5 (3.168 GHz to 3.696 GHz).

Previous experimental demonstrations have shown that a 1 meter wireless link produces similar results to the ones obtained using a 40 dB attenuator, which corresponds to the free-space air attenuation over 1 meter distance, approximately. Therefore, and for simplicity sake, the effect of the wireless link was simulated by the attenuator. In this experimental demonstration we have used two different PF-GI-POFs from Chromis Fiberoptics, namely, the GigaPOF-62LD and the GigaPOF-120LD, with core diameters of 62.5 μm, and 120 μm, respectively.

2.3. Experimental results and discussion

The experimental validation was carried out by transmitting data at bit rates of 53.3 Mbps, 200 Mbps and 480 Mbps.

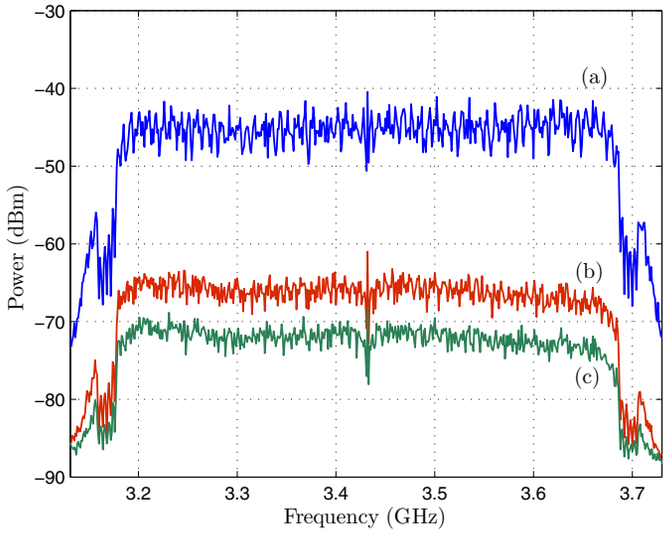
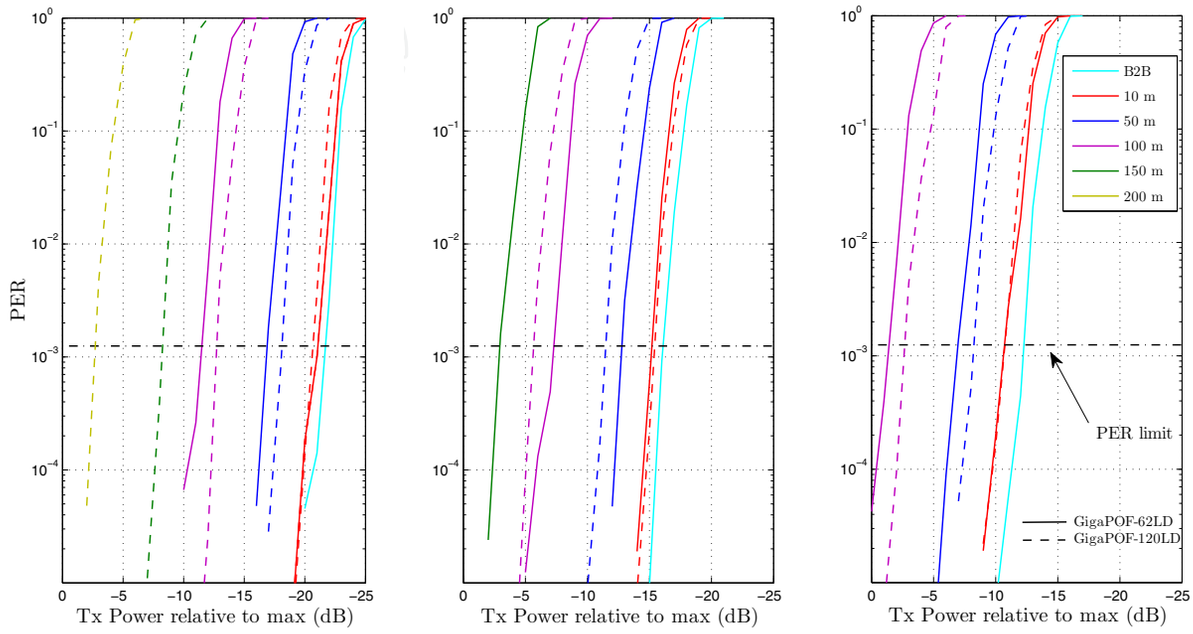


Figure 6. Spectrum of the MB-OFDM UWB signal (a) transmitted by the UWB kit and received after a 1 meter wireless link and (b) 50 meters and (c) 100 meters of GigaPOF-120LD (RBW = 1 MHz).

We also used a 64 octet packet length for PER measurements. Figure 6 shows the MB-OFDM UWB signal spectra obtained before the wireless link and after the GigaPOF-120LD. The

attenuation of these links obtained from equation (2) are 20.6 dB and 25.6 dB, which agrees with the measured values of 21 dB and 26 dB from Figure 6. In addition to the wireless/optical link attenuation, it can be seen that subcarriers suffer slightly different attenuations mainly due to the photodiode and amplifier frequency response. The UWB signal spectrum shows no distortion for the tested fiber lengths, which indicates that the bandwidth-distance product is not the factor limiting the transmission on the fiber.



(a) 53.3 Mbps. (b) 200 Mbps. (c) 480 Mbps.

Figure 7. PER vs. transmitted power after a 1 meter wireless link for transmission rates of 53.3, 200 and 480 Mbps for both GigaPOF-62LD and GigaPOF-120LD.

Figure 7 depicts the experimental results of PER as a function of transmitted power (relative to the maximum allowed value as defined by the ECMA-368 standard [12]) for different POF lengths preceded by a 1 meter wireless link and considering transmission rates of 53.3 Mbps, 200 Mbps and 480 Mbps. As expected, results show that the PER increases when the POF length is increased. The horizontal dashed line corresponds to a PER of 0.125 % which is the maximum PER allowed for a 64 octet frame body (ECMA-368 [12]).

Figure 8 shows the minimum required signal power (relative to the maximum) corresponding to the maximum allowed PER, as a function of POF length, where a 1 meter wireless channel is included. As expected, the PER increases for larger data rates, and the required power for achieving a valid transmission also increases.

A linearly increasing transmitted signal power (in dB) is necessary to compensate for the linearly increasing POF loss with distance, keeping both the receiver SNR and the PER constant, as indicated in Figure 8. This shows that the overall noise level is constant at the output of the receiver board, and that intermodulation products are sufficiently below the receiver noise level (for the chosen link parameters). A further interesting result is

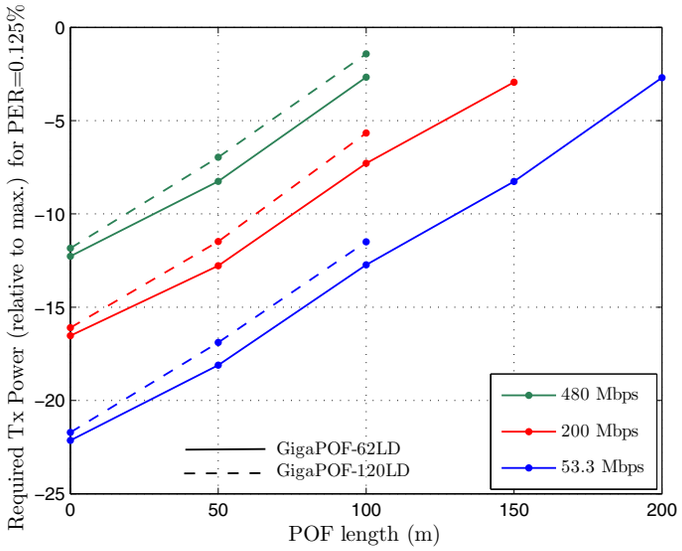
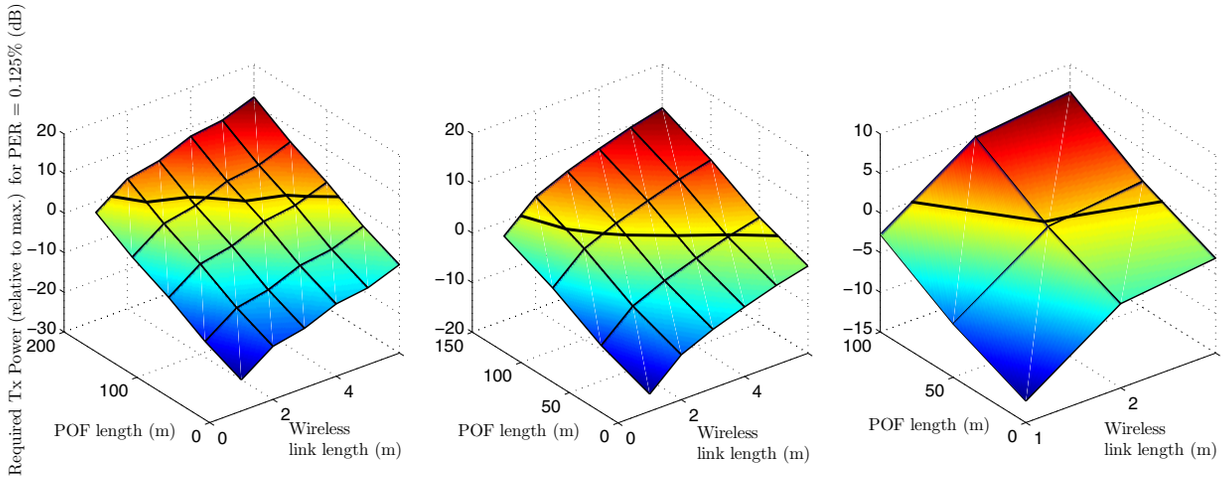


Figure 8. Required signal transmit power after 1 meter wireless link to achieve a PER of 0.125 % as a function of POF length for both GigaPOF-62LD and GigaPOF-120LD.



(a) 53.3 Mbps. (b) 200 Mbps. (c) 480 Mbps.

Figure 9. Required signal transmit power (relative to max.) to achieve a PER of 0.125% as a function of GigaPOF-120LD length and wireless link length for three different transmission rates.

that the slope of the plots depicted in Figure 8 correspond to the fiber attenuation, which is approximately 50 dB/Km in both cases, indicating that fiber attenuation (and not fiber bandwidth) is the dominant transmission penalty (see Figure 6).

Results also show that it is possible to transmit 480 Mbps up to 100 meters of POF when preceded by a 1 meter wireless link as well as 200 Mbps and 53.3 Mbps over 150 meters and 200 meters, respectively. The slight difference found in the back-to-back configuration shows that the large core diameter fiber has a better light coupling efficiency. This difference persists in all the POF lengths.

It was not possible to obtain results for fiber lengths longer than 100 meters, due to the unavailability of suitable GigaPOF-62LD cables at our lab. Nonetheless, by looking at the

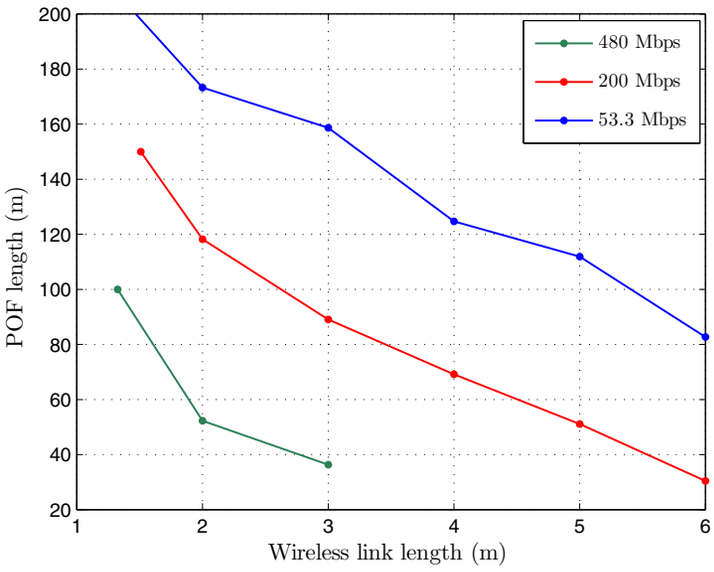


Figure 10. GigaPOF-120LD length vs. wireless link length when transmitting at the maximum allowed power for a 0.125 % PER.

plots trend, we can also infer that valid transmissions of 200 Mbps over 150 meters of GigaPOF-62LD and 53.3 Mbps over 200 meters of the same fiber, are likely achievable.

A generalization of the results plotted in Figure 8 is depicted in Figure 9 for the GigaPOF-120LD. In order to obtain these results, the required signal power for the PER of 0.125% was obtained for wireless links up to 6 meters (in one meter spans) in a back-to-back optical configuration. For the 10, 50 and 100 meters of GI-POF cases, results were extrapolated using the start point given by the back-to-back configuration and using the previous derived result that the transmission power increases linearly with the GI-POF length (see Figure 8). Note that the 1 meter wireless link results are the ones plotted in Figure 8. The solid black lines in Figure 9 indicate the intersection of the surface with the 0 dB plane, which represents the maximum transmitted power. Thus, combinations of POF and wireless links with required transmit powers above 0 dB are not allowed by the standard and their representation in the Figure result from the extrapolation used.

With this result it is possible to see that a 1 meter wireless link followed by a range extension of 150 meter of GI-POF requires the same amount of transmitted power as the 6 meter wireless link with a 30 meter GigaPOF-120LD link for a bitrate of 200 Mbps. Similarly, at 480 Mbps, we can see that 100 meters of GigaPOF-120LD preceded by a 1.3 meters wireless link gives the same performance as 3 meter wireless link followed by approximately 35 meters of fiber.

The specific cases given by the black lines in Figure 9, are represented in Figure 10. These results represent the maximum POF length as a function of the wireless link length when transmitting at the maximum allowed power for a 0.125 % PER.

In conclusion, results show that it is possible to transmit 200 Mbps over a 6 meter wireless link followed by 30 meters of GigaPOF-120LD. We have experimentally demonstrated maximum transmission distances of 150 meters and 200 meters, respectively, using GigaPOF-120LD,

with data rates of 200Mbps and 53.3 Mbps. It is also demonstrated that the PG-GI-POF attenuation, and not its bandwidth, is the dominant factor limiting the fiber link length.

3. UWB transmission in a radio-over-fiber system based on reflective electro-absorption modulators

As stated earlier, phase noise from optical sources is one of the factors impairing RoF system performance. Thus, very stable narrow linewidth optical sources are mandatory but also very expensive [15]. For the downlink signal transmission, an ultra-stable and common optical source can be used since it is located at the CS. However, in the uplink, it is not attractive in terms of complexity, size, power consumption and cost to have an optical source for each BSs. Furthermore, by eliminating the need of an optical source, BSs can be colorless and the wavelength assignment can be done at the CS.

Two main BS schemes are usually used in colorless RoF systems. The first scheme is based on an external modulator, photoreceiver and utilizes optical filtering techniques and wavelength reuse, or a more convenient method in which the optical carrier is remotely provided from the CS [16–18]. Another scheme of source free BSs is based on a single electro-absorption waveguide device in which a single component acts both as a modulator for the uplink and as photoreceiver for the downlink [19, 20]. Therefore, this transceiver device is a very attractive solution for a full-duplex RoF transmission.

Although an electro-absorption transceiver (EAT) based RoF system is simple and potentially has low power consumption, alternative solutions based on a dual lightwave approach and passive EATs have also been reported [21]. Using different wavelengths for segregating the uplink from the downlink optical paths makes it possible to minimize the transceiver insertion loss for both uplink and downlink signal transmission. Therefore, optical transceivers are increasingly considered as key components for the implementation of low-cost BSs [21].

The reflective EAM where the rear facet is coated with high reflection layer is an interesting device for operating simultaneously as a modulator and photoreceiver. In the following, the R-EAM performance as a transceiver in RoF systems is discussed. Additionally, an experimental evaluation of the R-EAM in terms of its slope efficiency (SE) and responsivity (R_e) at different wavelengths, optical powers and bias points is reported. Finally, a case study of UWB signal transmission is reported, where the optimum operation points are discussed for different scenarios: the bias for maximum SE and for maximum R_e are compared to zero bias.

3.1. R-EAM performance analysis

The experimental setup for the characterization of the 60 GHz R-EAM transceiver (CIP EAM-R-60-C-V-FCA) is shown in Figure 11.

Both electrical and optical test signals are used in order to obtain the electro-optical (E/O) and optical to electrical (O/E) response, which correspond to the slope efficiency and responsivity, respectively. We assume the decibel units for these variables to be obtained by $20\log_{10}(\cdot)$, as defined in the measurements of the laboratory equipment. Figure 12 shows the EO response

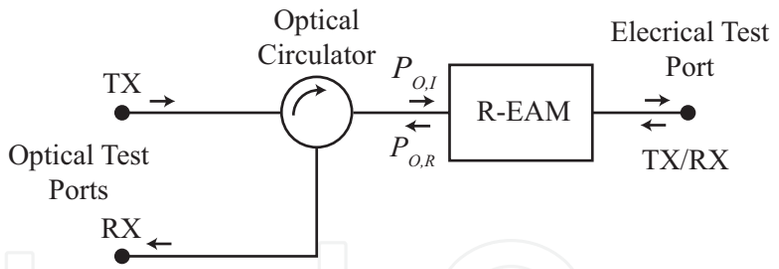
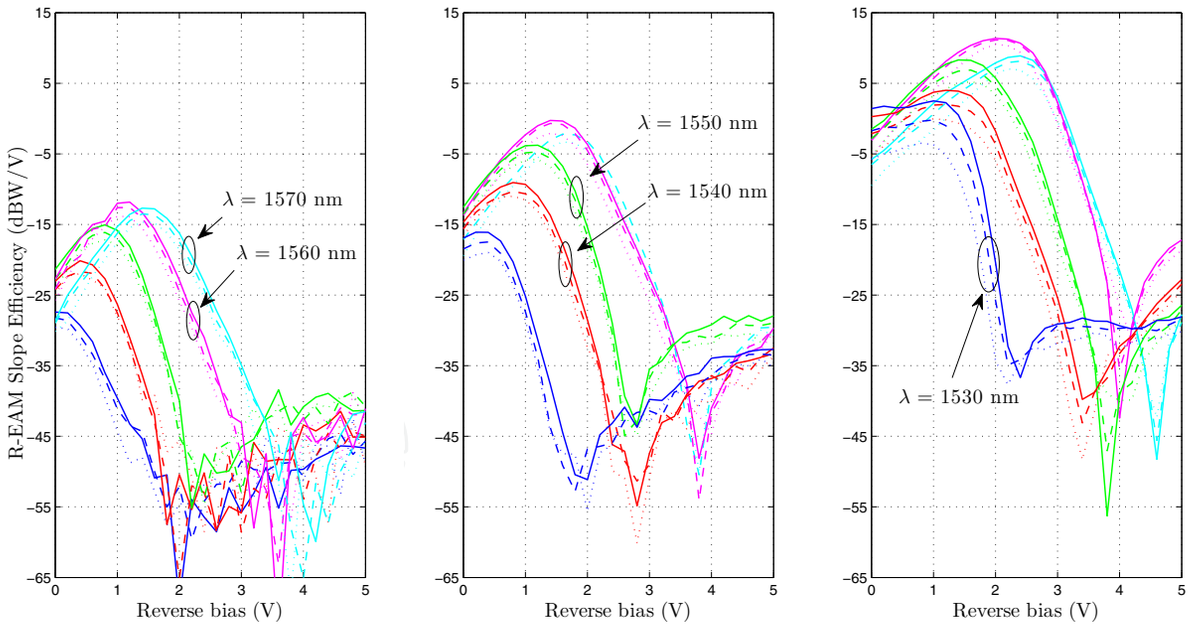


Figure 11. R-EAM characterization setup.

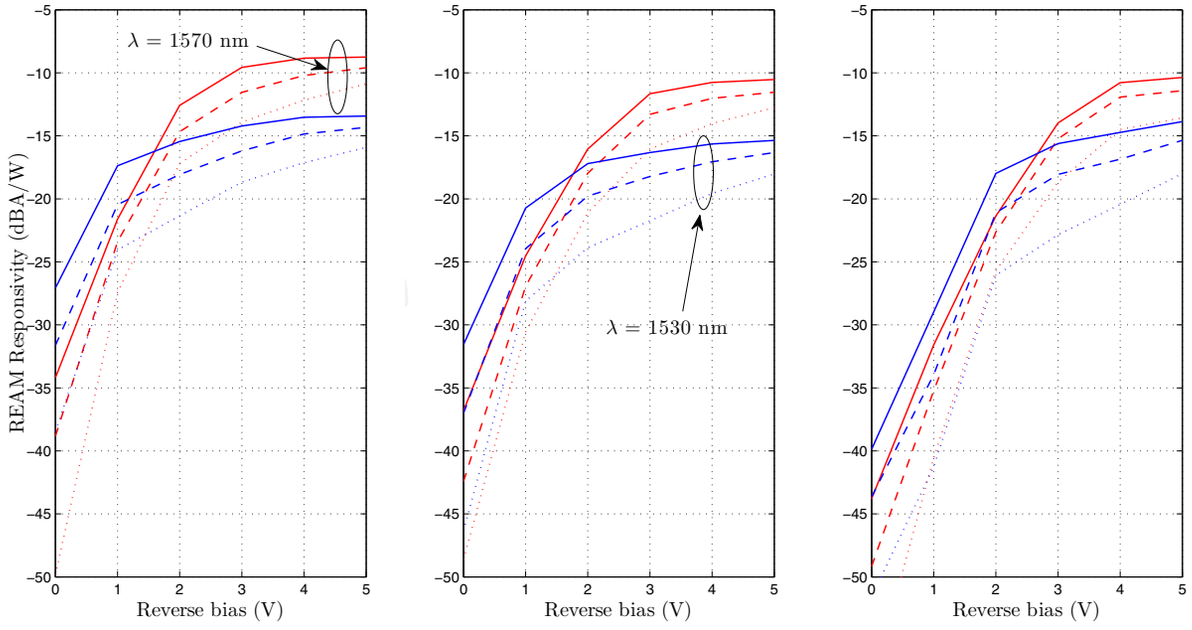
as a function of reverse bias voltage, for different frequencies and wavelengths. The R-EAM average optical input power, $P_{O,I}$, is varied by controlling the CW laser output power. It is apparent that the optimum bias voltage increases with both wavelength and the optical input power. It is also apparent that SE degrades slightly with frequency especially for high $P_{O,I}$, and lower wavelengths. Furthermore, it is easily seen that SE at the optimum bias voltage increases with $P_{O,I}$. Figure 13 shows the O/E response as a function of reverse bias voltage, for different frequencies and wavelengths. Due to the similarity of results, only two wavelengths are plotted, in order to allow a clear visualization. Similarly to what was observed for the E/O case, the responsivity degrades with frequency, particularly for high values of $P_{O,I}$, shorter wavelengths and decreasing reverse bias. Nevertheless, responsivity is shown to be more affected than SE. Furthermore, results also show that responsivity increases monotonically with reverse bias voltage.



(a) $P_{O,I} = -6$ dBm (b) $P_{O,I} = 0$ dBm (c) $P_{O,I} = 7$ dBm

Figure 12. E/O response vs. reverse bias voltage for different wavelengths and frequencies and optical input powers. Solid, dashed and dotted lines correspond to frequencies of 2.4, 5, 15 GHz, respectively.

The optimum bias points for maximum slope efficiency and responsivity have been extracted from the results of Figure 12 and 13. Considering these values, the R-EAM performance



(a) $P_{O,I} = -6\,\text{dBm}$ (b) $P_{O,I} = 0\,\text{dBm}$ (c) $P_{O,I} = 7\,\text{dBm}$

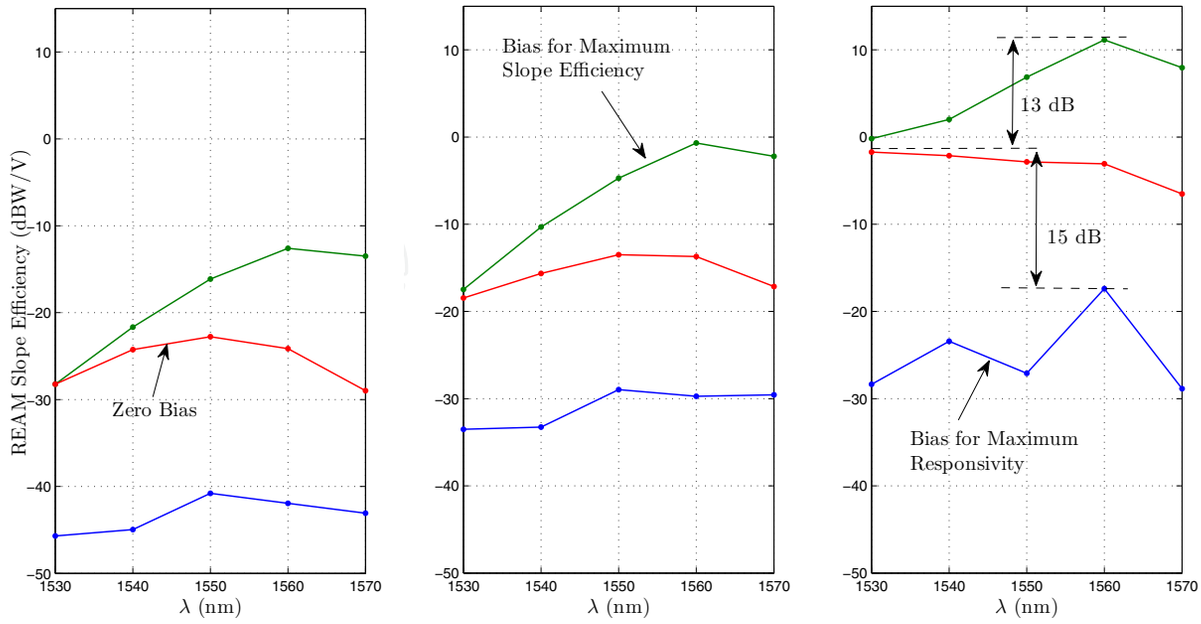
Figure 13. O/E response vs. reverse bias voltage for different wavelengths and frequencies and optical input powers. Solid, dashed and dotted lines correspond to frequencies of 2.4, 5, 15 GHz, respectively

is assessed in terms of slope efficiency and responsivity for the following cases: bias for maximum SE, bias for maximum R_e and zero bias. The results of this analysis are plotted in Figure 14 and 15.

The results in Figure 14 show that the best performance is obtained for a wavelength of 1560 nm, when the EAM is biased for maximum SE. However, when zero biased, the optimum wavelength is reduced to 1530 nm for $P_{0,I} = 7\,\text{dBm}$, where a penalty of 13 dB is incurred, compared to the case of maximum SE. Finally, when the EAM is biased for maximum responsivity, the optimum wavelength is 1560 nm and the SE decreases by 15 dB, compared to the zero bias case. It has also been verified experimentally that, as expected [18], the slope efficiency is proportional to the input optical power, as seen in Figure 14 (a) and (b), until it saturates at high optical powers, as shown by Figure 14 (c). Nevertheless, high optical input powers should be used in order to maximize the SE.

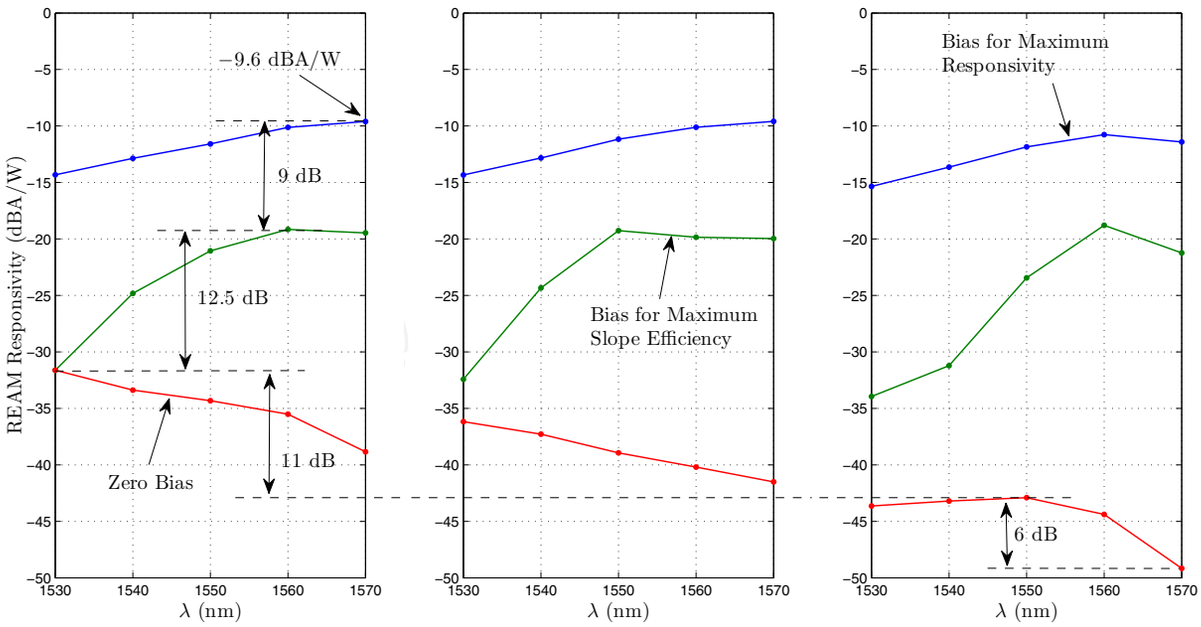
Concerning the EAM responsivity, its value is optimum for $P_{O,I} = -6\,\text{dBm}$, while a noticeable reduction is observed with increasing $P_{O,I}$, especially for zero bias. In both cases of biasing for maximum R_e and SE, the EAM responsivity improves with increasing wavelength, except for high $P_{O,I} = +7\,\text{dBm}$, where its maximum is achieved at $\lambda = 1560\,\text{nm}$.

The best responsivity values for both cases of biasing for maximum R_e and SE are $-9.6\,\text{dBA/W}$ and $-18.6\,\text{dBA/W}$, respectively. For the zero bias case, the responsivity decreases with wavelength for both input optical powers $-6\,\text{dBm}$ and $0\,\text{dBm}$, reaching a maximum of $-31\,\text{dBA/W}$ for $P_{O,I} = -6\,\text{dBm}$ and 1530 nm. However, for $P_{O,I} = +7\,\text{dBm}$ the responsivity is relatively constant with the wavelength, except for 1570 nm where it degrades by 6 dB. The



(a) $P_{O,I} = -6\,\mathrm{dBm}$ (b) $P_{O,I} = 0\,\mathrm{dBm}$ (c) $P_{O,I} = 7\,\mathrm{dBm}$

Figure 14. E/O response vs. wavelength for different bias configurations and optical input powers.



(a) $P_{O,I} = -6\,\mathrm{dBm}$ (b) $P_{O,I} = 0\,\mathrm{dBm}$ (c) $P_{O,I} = 7\,\mathrm{dBm}$

Figure 15. O/E response vs. wavelength for different bias configurations and optical input powers.

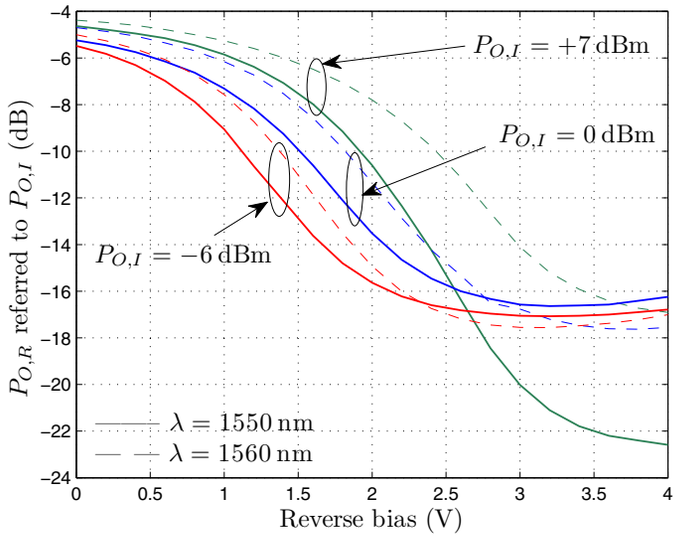


Figure 16. R-EAM reflected optical power, $P_{O,R}$ referred to the input optical power $P_{O,I}$.

responsivity degradation with increasing $P_{O,I}$, translates into a penalty of 11 dB when $P_{O,I}$ is increased from -6 dBm to $+7$ dBm.

The R-EAM performance was also assessed in terms of reflected optical power, $P_{O,R}$, for different values of input optical power $P_{O,I}$, the results of this analysis being shown in Figure 16. The reflected optical power is a relevant parameter with impact in the optical to electrical conversion. Therefore, this analysis considered the wavelengths of 1550 nm and 1560 nm, because these provide the best performance according to the measurements of slope efficiency given in Figure 15. The results given by the current analysis, indicate that the reflected optical power tends to decrease with increasing reverse bias voltage. Furthermore, the optical power reflected at the wavelength of 1550 nm is generally lower than that reflected at 1560 nm, except for higher reverse bias at low optical input powers.

3.2. System performance assessment

In this section, we consider the application of the R-EAM as a base station in a bidirectional transmission system, in a typical RoF network. A diagram of the application scenario is shown in Figure 17.

The RF downlink (DL) signal, generated by the CS transceiver (TRX) with a power of $P_{tx,DL}$, passes through an electrical circulator and amplifier with gain $G_{E,DL}$, and drives an E/O modulator, considered ideal in the present analysis. The optical downlink signal then passes through an optical circulator, and reaches the R-EAM through an optical fiber, with an incident optical power of $P_{O,I}$. The RF modulated optical signal is converted to the electrical domain by the R-EAM with a responsivity (R_e), and then reaches the mobile station through the wireless channel, which induces a signal loss of L. Note that the attenuation parameter L already includes both BS and MS antenna gains. Conversely, the RF uplink (UL) signal is generated by the mobile station transceiver with a power of $P_{tx,UL}$, and reaches the base station after being attenuated by the wireless link. The weak RF uplink signal can be amplified electrically ($G_{E,UL}$) before being converted from the electrical to the optical domain with a conversion

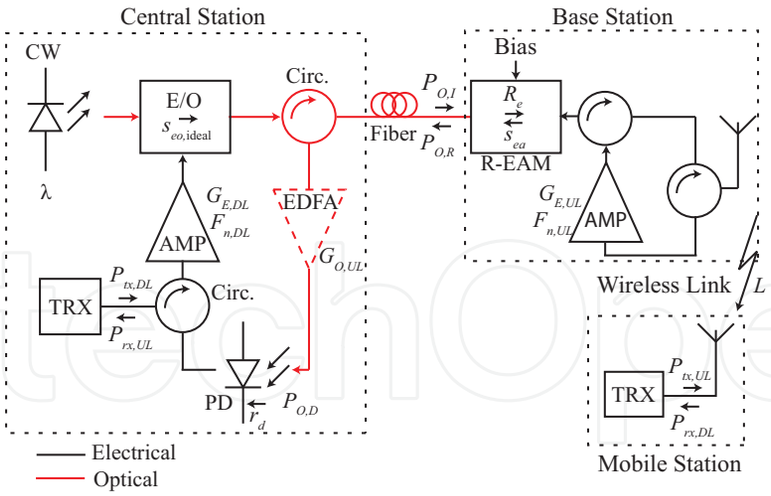


Figure 17. Considered setup for performance assessment. CW represents a continuous wave light source. Both TRX shown, represent the transceivers at the Control Station and Mobile Station. PD represents the Control Station photodiode. The EDFA depicted, represents an optional Erbium Doped Fiber Amplifier.

efficiency given by the EAM slope efficiency, s_{ea}, by modulating the reflected optical carrier with power $P_{O,R}$. The uplink signal might be further optically ($G_{O,UL}$) amplified before reaching the CS transceiver. This optical amplification is only adequate if the optical power is low (typically less than -3 dBm), so that the noise added by the EDFA is still below the noise level at the receiver [22]. In the following analysis, we assume $P_{O,R} \cong P_{O,D}$, since the optical circulator loss and the use of an EDFA are not considered. The metric used to evaluate performance of the system is the signal to noise ratio (SNR).

The SNR of the RF signal arriving at the mobile station can be written as:

$$\mathrm{SNR}_{rx,MS} = \frac{\langle I_{rx,DL}^2 \rangle}{\sigma_{n,MS}^2} = \frac{\langle I_{tx,DL}^2 \rangle G_{DL}}{\langle I_{t,MS}^2 \rangle} \tag{3}$$

where,

$$G_{DL} = G_{E,DL} s_{eo,\mathrm{ideal}}^2 R_e^2 L \tag{4}$$

$$\langle I_{t,MS}^2 \rangle = (4T + T_a) k \Delta_f / R_{MS} + (F_{n,DL} - 1) k T G_{DL} \Delta_f / R_{EO} \tag{5}$$

$$P_{tx,DL} = R_{CS} \langle I_{tx,DL}^2 \rangle \tag{6}$$

Therefore, the SNR at the receiver can be written as the following ratio:

$$\mathrm{SNR}_{rx,MS} = \frac{(P_{tx,DL}/\Delta_f) G_{DL}/R_{EO}}{(4T + T_a) k/R_{MS} + (F_{n,DL} - 1) k T G_{DL}/R_{EO}} \tag{7}$$

where R_{MS} represents the impedance of the mobile station circuitry, R_{EO} the impedance of the E/O converter circuitry, Δ_f the transmission bandwidth, $s_{eo,\mathrm{ideal}}$ the slope efficiency of the ideal E/O modulator, $F_{n,DL}$ the noise factor of the electrical amplifier that precedes the

modulator, k is Boltzmann's constant, $T = 290\,\mathrm{K}$ and $T_a = 120\,\mathrm{K}$ is the antenna temperature. Since the link gain (G_{DL}) is low, the noise at the receiver is dominated by the thermal noise of the receiver circuitry itself. Furthermore, since the R-EAM efficiency is higher in the downlink, regardless of the bias conditions, the SNR is considerably higher than in the uplink.

The SNR of the RF signal arriving at the CS can be written as:

$$\mathrm{SNR}_{rx,CS} = \frac{\langle I_{rx,UL}^2 \rangle}{\sigma_{n,CS}^2} = \frac{\langle I_{tx,UL}^2 \rangle G_{UL}}{\langle I_{rin}^2 \rangle + \langle I_{sn}^2 \rangle + \langle I_{t,CS}^2 \rangle} \tag{8}$$

where,

$$G_{UL} = G_{E,UL} s_{ea}^2 R_e^2 L \tag{9}$$

$$\langle I_{rin}^2 \rangle = r_d^2 \langle P_{O,D} \rangle^2 10^{\mathrm{RIN}/10} \Delta_f \tag{10}$$

$$\langle I_{sn}^2 \rangle = 2 q r_d \langle P_{O,D} \rangle \Delta_f \tag{11}$$

$$\langle I_{t,CS}^2 \rangle = 4kT\Delta_f / R_{\mathrm{L}} + (T_a + (F_{n,UL} - 1)T) k G_{E,UL} s_{ea}^2 r_d^2 \Delta_f / R_{EAM} \tag{12}$$

$$P_{tx,UL} = R_{MS} \langle I_{tx,UL}^2 \rangle \tag{13}$$

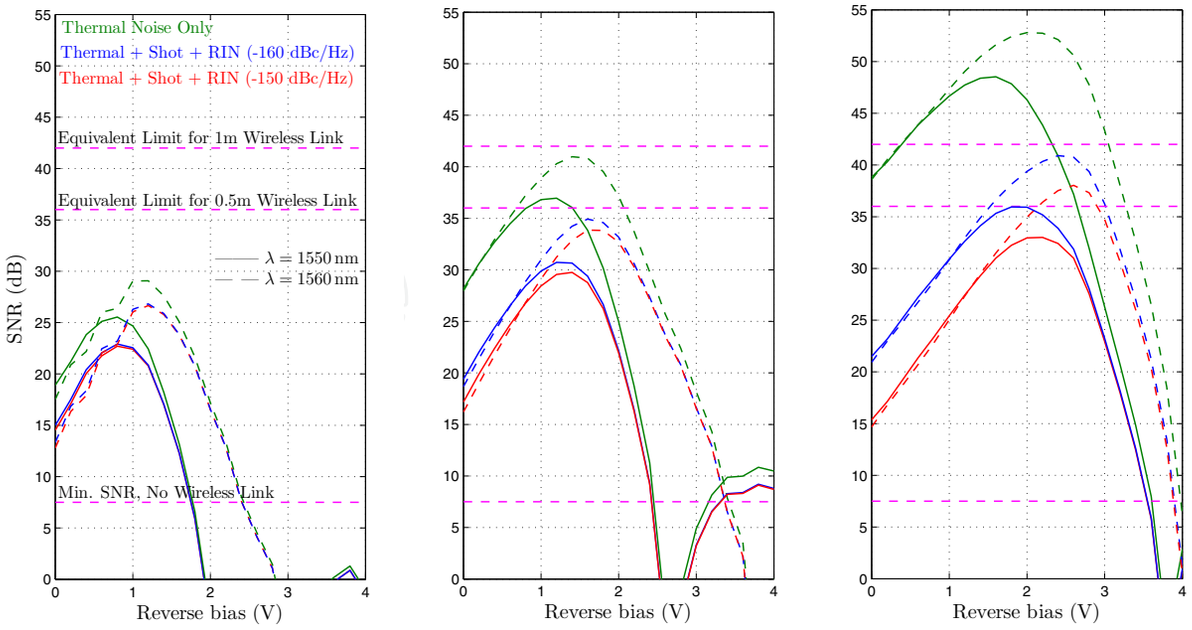
where R_{EAM} represents the impedance of the R-EAM circuitry.

The noise terms are referred to the photodiode output, and stem from three main components: the relative intensity noise (RIN) from the laser source (proportional to the square of $\langle P_{O,D} \rangle$), the shot noise (proportional to $\langle P_{O,D} \rangle$), and the last term is the thermal noise from both the photodiode load (R_{L}), the antenna and the uplink electrical amplifier, where $F_{n,UL}$ is the noise factor of the amplifier at the base-station. The thermal noise from the electrical transmitter at the mobile station can be neglected, due to the low total gain of the link (G_{UL}). The optical power detected by the photodiode, $P_{O,D}$, is expected to have a significant impact on the noise contribution at the receiver. In the presented results, the wireless channel attenuation (L) was not considered, the fiber is considered ideal, $G_{E,UL/DL} = 1$, $F_{n,UL/DL} = 1$, $R_{\mathrm{L}} = 1000\,\Omega$ and $R_{MS/EO/EAM} = 50\,\Omega$.

3.3. UWB-over-fiber results and discussion

The present analysis considers again the usage of typical UWB transceivers (*Wisair DVK9110*), which operate in band group 1 (from 3.168 GHz to 4.752 GHz) and have a maximum transmission power of approximately $P_{tx,UL}/\Delta_f = -45.3\,\mathrm{dBm}$, when the MS antenna gain (considered to be 4 dB) is lumped into the wireless channel attenuation.

The UWB receiver sensitivity of $-70.4\,\mathrm{dBm}$ at 480 Mbit/s specified in the standard [12], is not valid for an optical front-end. This value assumes a typical value of noise level in a wireless receiver of $-80.5\,\mathrm{dBm}$, which indicates that a receiver should be able to meet the target performance specified in the standard for a SNR of approximately 10 dB. In the present



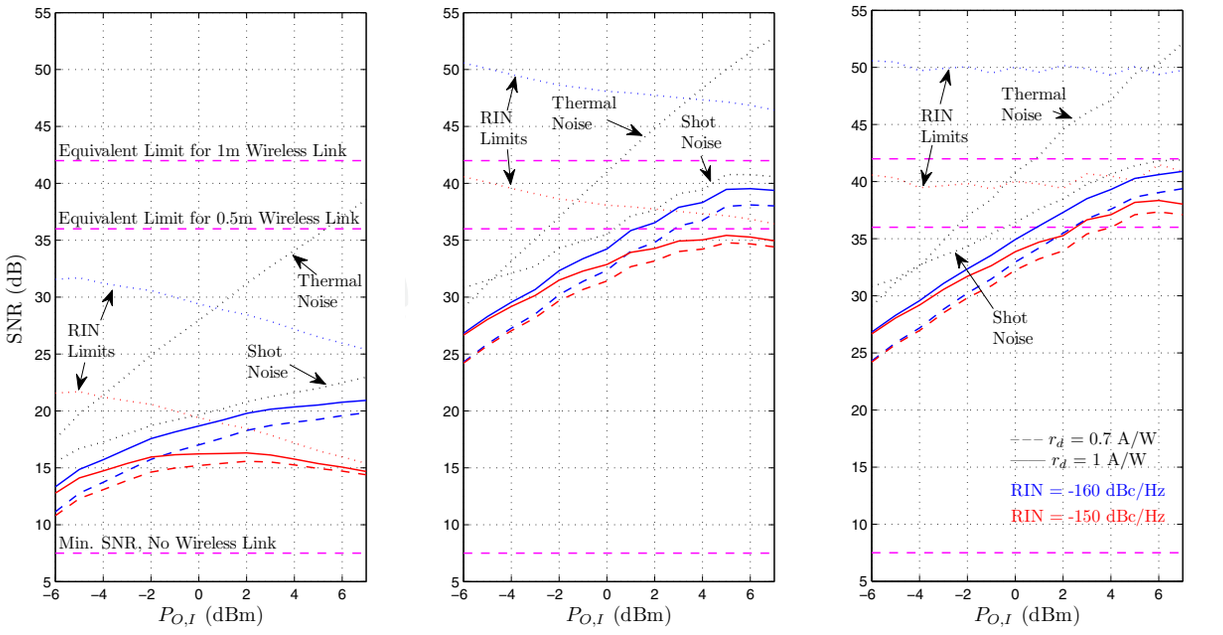
(a) $P_{O,I} = -6\,\text{dBm}$ (b) $P_{O,I} = 0\,\text{dBm}$ (c) $P_{O,I} = 7\,\text{dBm}$

Figure 18. SNR as a function of reverse bias for three different values of optical input power.

analysis, a minimum SNR of 7.5 dB is considered, which has been measured experimentally for the mentioned commercial UWB transceiver.

The results in Figure 18 show the SNR as a function of the reverse bias, for three different values of $P_{O,I}$, (a) -6 dBm, (b) 0 dBm and (c) $+7$ dBm, considering a responsivity of 1 A/W and two different wavelengths, 1550 nm and 1560 nm and RIN values, -150 dB/Hz and -160 dB/Hz. Moreover, SNR results considering only the thermal noise term are also depicted for comparisson purposes. Two additional equivalent SNR limits that consider a wireless link length of 0.5 m and also 1 m are also shown in the results, which account for a signal loss of 28.5 and 34 dB at 4 GHz, respectively, when considering a total gain of the antennas of 10 dBi, among MS and BS. Results show that for low reverse bias the impact of both shot noise and RIN increase with the incident optical power. This result comes in line with the ones of the reflected optical power plotted in Figure 16. Moreover, it is clearly seen that the SNR is optimum for a wavelength of 1560 nm with a maximum SNR 5 dB better than that at 1550 nm, although slightly worse for zero bias.

In Figure 19 the SNR is obtained as a function of $P_{O,I}$, for the following cases: (a) zero bias, (b) optimum bias for maximum SE and (c) optimum bias for maximum SNR, considering only the wavelength of 1560 nm. Again, two additional equivalent SNR limits that consider a wireless link length of 0.5 m and also 1 m are also shown in the results. The results considering optimum bias for maximum Slope Efficiency are, at the maximum points, $5-6$ dB worse than those for maximum SNR, essentially because there is a compromise between signal power, which is affected by the $s_{e,a}$ as a function of bias voltage, and noise power, affected by the $P_{O,D}$ which also depends on the bias voltage.



(a) Zero bias (b) Optimum bias for maximum SE (c) Optimum bias for maximum SNR

Figure 19. SNR as a function of optical input power for thre different bias cases.

From an overview perspective, it can be noted that the SNR performance increases with $P_{O,I}$ for a RIN of $-160\,\mathrm{dB/Hz}$, whereas for $-150\,\mathrm{dB/Hz}$ there is an optimum value of $P_{O,I}$ for maximum SNR. At zero bias, a maximum margin of 9 dB compared to the UWB SNR limit is obtained with a laser RIN of $-150\,\mathrm{dB/Hz}$ for a $P_{O,I}$ of $\sim$0 dBm, whereas for a RIN of $-160\,\mathrm{dB/Hz}$ the performance becomes limited by shot noise, allowing for a SNR margin of $\sim$ 13.5 dB. However, the results indicate that none of such limits are achieved at zero bias, because of both RIN and shot noise limitations, which means that a totally passive base-station is not practicable, for reasonable wireless link distances. Results for optimum bias for maximum SE indicate that the SNR for a RIN of $-150\,\mathrm{dB/Hz}$ practically achieves the UWB SNR limit for a wireless link distance of 0.5 meters with a $P_{O,I}$ of $\sim$6dBm, whereas for a RIN of $-160\,\mathrm{dB/Hz}$ a 1 meter link is almost achieved. Note that while the former SNR is limited by the RIN term, the latter is limited by the shot noise. At optimum bias for maximum SNR, a margin of 33.5 dB is obtained at the maximum $P_{O,I}$, for a RIN of $-160\,\mathrm{dB/Hz}$ and $R_e = 1\,\mathrm{A/W}$, allowing for an acceptable wireless link distance of approximately 1 meter. For a RIN of $-150\,\mathrm{dB/Hz}$, there is enough SNR margin to allow for a wireless link distance between 0.5 and 1 meter. Furthermore, by reducing the UWB throughput, a maximum distance of 2.8 meters would be achievable at 53.3 Mbit/s, at a minimum SNR of 0 dB. Since the R-EAM slope efficiency at optimum bias for maximum responsivity is worse than that at zero bias, there is no advantage in analyzing that scenario.

In conclusion, the optimum operation point was found to be the biasing for maximum SNR using an high optical input power and a wavelength of 1560 nm. Although a zero bias configuration is an attractive technique, it is not suitable to provide a reasonable wireless link distance for UWB. Additionally, we also conclude that one of the performance-limiting

factors comes from the laser RIN that imposes a limit on the achievable SNR, especially for a zero biased modulator. A laser RIN of −160 dB/Hz would be required in order to avoid the RIN limitation. In this case the performance becomes limited by shot noise. Although a zero bias configuration is an attractive technique, it is not suitable to provide a reasonable wireless link distance for UWB signals.

4. Conclusions

This chapter presented a study of the transmission performance of UWB signals over two different optical based networks. Firstly, a low-cost RoF solution based on a VCSEL and two high performance POFs for assessing the UWB signal transmission performance was presented. Experimental measurements of packet error rate (PER) and minimum transmitted powers to achieve the maximum allowed PER showed that it is possible to have a viable transmission at data rates of 480 Mbps, 200 Mbps and 53.3 Mbps over 100, 150 and 200 meters of PF-GI-POF, respectively, preceded by a 1 meter wireless link. The two PF-GI POFs have diameters of 62.5 μm and 120 μm with bandwidth distance products higher than 1 GHz·Km.

It was shown that the PF-GI-POF attenuation, and not its bandwidth, is the dominant factor limiting the fiber link length. Therefore, the PF-GI-POFs are a viable solution for transporting UWB signals. In particular, the larger core GI-POF with 120 μm diameter may find applications in both the home and office environments where easiness of installation and handling are vital.

Finally, a performance analysis of both the slope efficiency and responsivity of a R-EAM transceiver for different wavelengths, optical powers and bias points was presented. In particular, the performance of RoF transmisssion with zero bias transceivers was evaluated for the UWB ECMA-368 standard. The optimum operation point was found to be the biasing the transceivers for maximum link SNR, using a high optical input power at 1560 nm wavelength. Although a zero bias may seem limitative, the R-EAM can be optimally biased using a small battery, which can last for several months, allowing the BS to operate almost as a passive device.

Acknowledgments

This work was supported in part by EC Framework 7 (FP7) project DAPHNE (www.fp7daphne.eu) – Developing aircraft photonic networks (grant ACP8-GA-2009-233709). We acknowledge funding from FCT and program POCTI/FEDER under the National Plan for Scientific Hardware Renewal with grant REEQ/1272/EEI/2005. D. Coelho also acknowledges support from FCT through a PhD grant.

Author details

João M.B. Oliveira, Diogo Coelho and Henrique M. Salgado
Faculdade de Engenharia da Universidade do Porto
Instituto de Engenharia de Sistemas e Computadores do Porto - INESC TEC, Portugal

Luís M. Pessoa and Jorge C.S. Castro
Instituto de Engenharia de Sistemas e Computadores do Porto - INESC TEC, Portugal

5. References

[1] Federal Communications Commission. First report and order, revision of part 15 of commission's rule regarding ultra-wideband transmission system. FCC 02-48, 22:2, 2002.

[2] JE Mitchell. Performance of OFDM at 5.8 GHz using radio over fibre link. *IEEE Electronics Letters*, 40(21):1353–1354, 2004.

[3] Pak Kay Tang, Ling Chuen Ong, A. Alphones, B. Luo, and M. Fujise. PER and EVM measurements of a radio-over-fiber network for cellular and WLAN system applications. *IEEE Journal of Lightwave Technology*, 22(11):2370 – 2376, 2004.

[4] N.J. Gomes, M. Morant, A. Alphones, B. Cabon, J.E. Mitchell, C. Lethien, M. Csörnyei, A. Stöhr, and S. Iezekiel. Radio-over-fiber transport for the support of wireless broadband services [invited]. *Journal of Optical Networking*, 8(2):156–178, 2009.

[5] M. Jazayerifar, B. Cabon, and J.A. Salehi. Transmission of multi-band OFDM and impulse radio ultra-wideband signals over single mode fiber. *IEEE Journal of Lightwave Technology*, 26(15):2594–2603, 2008.

[6] M. Sauer, A. Kobyakov, and J. George. Radio over fiber for picocellular network architectures. *IEEE Journal of Lightwave Technology*, 25(11):3301–3320, 2007.

[7] C. Lethien, C. Loyez, J.P. Vilcot, L. Clavier, M. Bocquet, and P.A. Rolland. Indoor coverage improvement of mb-ofdm uwb signals with radio over pof system. *Optics Communications*, 282(24):4706–4715, 2009.

[8] O. Ziemann, H. Poisel, and J. Vinogradov. Potential of high speed, short distance optical data communication on large diameter optical fibers. In *Proc. 1st Electronics Systemintegration Technology Conf*, volume 1, pages 409–414, 2006.

[9] A. Polley, R. J. Gandhi, and S. E. Ralph. 40gbps links using plastic optical fiber. In *Proc. Conf. Optical Fiber Communication and the National Fiber Optic Engineers Conf. OFC/NFOEC 2007*, pages 1–3, 2007.

[10] T. Ishigure, Y. Aruga, and Y. Koike. High-bandwidth pvdf-clad gi pof with ultra-low bending loss. *Journal of Lightwave Technology*, 25(1):335–345, 2007.

[11] T. Kibler and E. Zeeb. Optical data links for automotive applications. In *Electronic Components and Technology Conference, 2004. Proceedings. 54th*, volume 2, pages 1360–1370. IEEE, 2004.

[12] S. ECMA. Ecma-368: High rate ultra wideband phy and mac standard, 2005.

[13] X. N. Fernando and A. Anpalagan. On the design of optical fiber based wireless access systems. In *Proc. IEEE Int Communications Conf*, volume 6, pages 3550–3555, 2004.

[14] T. Marozsak and E. Udvary. Vertical cavity surface emitting lasers in radio over fiber applications. In *Proc. MIKON-2002 Microwaves, Radar and Wireless Communications 14th Int. Conf*, volume 1, pages 41–44, 2002.

[15] C. Lim, A. Nirmalathas, M. Bakaul, P. Gamage, K.L. Lee, Y. Yang, D. Novak, and R. Waterhouse. Fiber-wireless networks and subsystem technologies. *IEEE Journal of Lightwave Technology*, 28(4):390–405, 2010.

[16] Z. Jia, J. Yu, and G.K. Chang. A full-duplex radio-over-fiber system based on optical carrier suppression and reuse. *IEEE Photonics Technology Letters*, 18(16):1726–1728, 2006.

[17] L. Chen, H. Wen, and S. Wen. A radio-over-fiber system with a novel scheme for millimeter-wave generation and wavelength reuse for up-link connection. *Photonics Technology Letters, IEEE*, 18(19):2056–2058, 2006.

[18] C.H. Cox. *Analog optical links: theory and practice*. Cambridge Univ Pr, 2004.
[19] D. Wake, D. Johansson, and DG Moodie. Passive picocell: a new concept in wireless network infrastructure. *IEEE Electronics Letters*, 33(5):404–406, 1997.
[20] A. Stohr, K. Kitayama, and D. Jager. Full-duplex fiber-optic RF subcarrier transmission using a dual-function modulator/photodetector. *IEEE Transactions on Microwave Theory and Techniques*, 47(7):1338–1341, 1999.
[21] K.I. Kitayama. Architectural considerations of fiber-radio millimeter-wave wireless access systems. *Fiber and Integrated Optics*, 19(2):167–186, 2000.
[22] G. Keiser. *Optical fiber communications*. Wiley Online Library, 2000.

IntechOpen